Impact of transient groundwater storage on the discharge of Himalayan rivers

Christoff Andermann[1,2], Laurent Longuevergne[1], Stéphane Bonnet[3], Alain Crave[1], Philippe Davy[1] and Richard Gloaguen[2]

[1] Géosciences Rennes, Université de Rennes 1, CNRS, Campus de Beaulieu, 35042 Rennes, France

[2] Remote Sensing Group, Geology Institute, TU Bergakademie Freiberg, B.-von-Cotta-Str. 2, 09599 Freiberg, Germany

[3] Géosciences Environnement Toulouse, Université de Toulouse, CNRS-UPS-IRD, Observatoire Midi-Pyrénées, 14 Av. Edouard Belin, 31400 Toulouse, France

Corresponding author:

Christoff Andermann,

Tel (+33) 2 23 23 66 24

christoff.andermann@univ-rennes1.fr

The transfer of precipitation into rivers involves temporary water storage in reservoirs[1,2] such as soils, groundwater, snow and glaciers, where different residence times influence the hydrological cycle. In the central Himalayas, the water budget is considered to be primarily controlled by monsoon rainfall, snow and glacier melt[3,4], and secondarily by evapotranspiration[3]. The existence of a deep groundwater contribution[5-7] is deduced from the chemistry of Himalayan rivers[6]. However, its importance in the annual water budget remains to be evaluated. Here, we analyze ~30 years of daily precipitation and discharge within major catchments in Nepal. We observe annual precipitation-discharge hysteresis loops, in both glaciated and unglaciated catchments, independently of the geological setting. This implies the temporal storage of water in

a reservoir whose characteristic response time (~45 days) represents a typical diffusivity (~1 $m^2 s^{-1}$) of fractured basement aquifers[8]. This transient storage capacity is of ~28 km^3 for the three main catchments of Nepal, whereas we estimate snow and glacier melt contribution to be ~14 $km^3 yr^{-1}$ (~10% of the annual river discharge). We conclude that groundwater storage in fractured basement constitutes an important compartment of the Himalayan river discharge cycle, that can be quantified through the study of precipitation and discharge throughout the year.

The discharge of the central Himalayan rivers is governed by a strong precipitation seasonality [3,6,9,10] (Fig. 1) with up to 80% of the annual rainfall occurring during the Indian Summer Monsoon (ISM) season[3]. The ISM precipitation is the main source for glacier mass accumulation[9] and its spatial distribution is strongly influenced by orographic effects[3]. Variations in intensity and duration of the ISM, linked to El Nino/Southern Oscillation (ENSO)[11], enhance the annual amount of precipitation by ~25 to 50% with respect to the annual mean at low to moderate elevation (>3 km), and up to 200% at high elevation[12]. Snowmelt contributes to a significant fraction of river discharge in the western and eastern Himalayas and on the Tibetan plateau[3,13], but only to a minor fraction (~10%) in the central Himalayas, mainly in the early ISM (May to July)[3]. It has been suggested that rainfall-derived discharge, ice and snowmelt are the primary factors controlling Himalayan river discharge, with evapotranspiration forming a secondary minor component[3]. Notwithstanding, this hydrological budget model neglects transient water storage in soils, floodplains and groundwater. However, geochemical data indicate that a non-negligible part of surface runoff originates from deep groundwater reservoirs[6].

We investigate the transfer of water within the main catchments of the Nepal Himalayas (Fig. 1a) using a daily meteorological and hydrological dataset spanning ~30 years (Table 1). We consider the three main catchments of Nepal (Sapta Koshi, Narayani and Karnali basins), some of their tributaries, and three unglaciated small catchments at the front of the Himalayan range (Fig. 1a and Table 1). The main catchments drain the entire Himalayan range of Nepal, from the Tibetan Plateau to the Lesser Himalayas. Most of their headwaters are located on the arid Plateau (Fig. 1a), characterized

by a weaker influence of the ISM. The rivers incise bedrock comprising, from north to south, the low-grade Paleozoic-Mesozoic Tethyan Sediment Series, high-grade metamorphic gneisses and migmatites of the High Himalayan Crystalline Series and low-grade Proterozoic sediments of the Lesser Himalayas (Fig. 1c). Most of the data considered here come from outlet stations located to the north of the Siwalik foreland. The annual specific discharge of the studied basins is typically on the order of ~10^3 mm yr^{-1} (Table 1) and their annual hydrograph clearly shows the seasonal impact of the ISM on river discharge, generally peaking in July/August[3,14] (Fig. 1b). Mean annual basin precipitation is 920, 1396 and 920 mm yr^{-1} in the Sapta Koshi, Narayani and Karnali catchments, respectively. However, precipitation is spatially heterogeneous (Fig. 1a) and is strongly controlled by orography, reaching a maximum between elevations of 2 to 3 km[15,16]. The upper parts of the catchments are glaciated (Fig. 1a), covering between 4 and 15 % of the catchment area (Table 1).

We calculated mean basin-wide daily precipitation rate and use daily discharge measurements to compute specific water discharge for all the studied drainage basins (see Methods). Plots of daily precipitation vs. specific discharge highlight a considerable scatter within the ~30 year dataset (Fig. 2a). However, the chronology of the data exhibits a well-defined annual cycle, showing an increase of discharge with increasing precipitation during pre-ISM (March-May) to ISM (June-September) and a decrease during post-ISM (October-November). The systematic higher discharge for a given precipitation rate during post-ISM compared with pre-ISM is striking. The data consequently shows an annual anticlockwise hysteresis loop (Fig. 2a). A 30-day moving average highlights the temporal consistency of the loop from year to year (Fig. 2a, inset). Data scattering results from inter-annual variability, particularly during post-ISM, as illustrated by comparing the data during a strong or a weak ISM year (see Supplementary Fig. S1). The annual anticlockwise hysteresis loop is observed in all studied basins (Fig. 2b), regardless of the geological units, the presence of glaciers or snow cover (Tab. 1).

Anticlockwise hysteresis loops imply that precipitation is temporarily stored within the catchments and not transferred directly to the river during pre-ISM and ISM seasons, whereas the

storage compartment is drained during post-ISM. Glaciers can be directly ruled out as the main contributor to the observed hysteresis effect because the release of water by glacier or snow melt occurs principally during pre-ISM to ISM season[3,13] (Fig. 3b and S2), which is not consistent with the anticlockwise nature of the hysteresis. Moreover, hysteresis effects are observed in both glaciated and unglaciated catchments (Fig. 2b). As the potential evapotranspiration in the Himalayas reaches a maximum during pre-ISM, in April-May[17] (Fig. 1b), this could qualitatively explain the anticlockwise hysteresis loop. However, it is estimated to account for less than 10% of the overall hydrological budget[3], so this effect plays likely a minor role, mainly because the magnitude of evapotranspiration rapidly decreases with elevation[17]. Consequently, the main mechanism explaining the hysteresis effect is likely a transient storage of water in a groundwater unit during the rising ISM and its post-ISM release.

To precise the role of groundwater storage on the Himalayan hydrological cycle, we solved the water balance at catchment scale in order to discriminate time response distribution in discharge data and relate it to storage compartments via hydrological modeling. We used a modified version of the conceptual hydrological model GR2M (see Methods), which addresses several physical processes in a simplified, but proven robust, way in a wide range of climatological settings[18]. Because the observed hysteresis effect is a seasonal process, daily modeling of hydrological processes is not the pertinent scale for our purpose (see ref. 19). The large diversity of involved processes, within a wide range of environmental settings, limits the reliability of short-term modeling so we modeled the data at a monthly rather than at a daily scale. Note, that we nevertheless tested daily scale modeling (see Methods and Supplementary Table S1). Modeled daily results are generally similar to monthly ones (Table 1), but the efficiency is however less well described (Table 1 and Supplementary Table S1). The model simulates the catchment response to rainfall in terms of river discharge and incorporates three components (see supplementary figure S3): 1) a snow module based on the HBV approach[20] (see Methods), 2) a fast rain-to-discharge flow related to quick runoff processes, and 3) a slow flow component representing groundwater contribution. This third reservoir retards the rain-discharge response and yields baseflow during dry periods. It is characterized by a response time t_c, defined as

111 the time for a hydrological system to reach equilibrium after the hydraulic head has changed[1]. The
112 model is forced by precipitation, temperature and potential evapotranspiration (see Methods). We
113 calibrated on the logarithm of all the observed daily water discharge to account for the large range of
114 discharges, *i. e.* to apply identical weights to both high and low water stages, and under the constraint
115 that total observed and modeled discharge volumes are identical. The modeling is robust in most
116 catchments: hysteresis loops are confidently reproduced for all catchments (e. g. Supplementary Fig.
117 S4) with Nash-Sutcliffe coefficients of 0.89, 0.91 and 0.92 for Sapta Koshi, Narayani and Karnali
118 basins, respectively (Table 1). The modeling implies a significant storage of water within the slow
119 flow reservoir, with calculated t_c longer than one month (Table 1). Modeled data are in agreement with
120 t_c values derived directly from the fit of baseflow recession curves[21] (see Methods and Table 1). This
121 delay between precipitation and discharge yields baseflow during dry periods and is responsible for
122 the existence of the hysteresis loops. Shorter t_c, associated with a low storage capacity (e.g. 10 days
123 equivalent to 20 times smaller storage capacity), do not allow to reproduce the observed hysteresis
124 loops analytically (see Methods and Supplementary Fig. S5c).
125
126 The nature of the groundwater system controlling the hysteresis effect is provided by its
127 response time t_c. For groundwater systems, t_c is inversely proportional to the hydraulic diffusivity D
128 (transmissivity divided by storage coefficient) and is proportional to the square of the characteristic
129 aquifer scale L_c: $t_c \sim L_c^2 * D^{-1}$ ref 1. L_c is the characteristic distance between the aquifer and streams, which
130 is approximately the hillslope length if aquifers are spread homogeneously over the drainage basin.
131 Considering L_c in the range 0.5–5 km and t_c, of ~45 days, equivalent diffusivity values are about ~1 m^2
132 s^{-1}, a typical value of aquifers in fractured rocks[8] (0.01 to 10 m^2 s^{-1}). Recession curve exponents
133 calculated on the falling limb of the post-ISM hydrograph (see Methods) are close to 1, and suggest
134 the contribution of a confined aquifer to discharge[21]. The estimated aquifer storage capacity is ~180
135 mm per unit area, representing ~28 km^3 for the three main catchments of Nepal (Table 1). Modeling
136 also indicates that the annual volume of water flowing through this groundwater system represents
137 ~2/3 of the annual river discharge (Supplementary Table S1). The modeled storage dynamics matches
138 the groundwater table variations observed in dug-wells, e.g. in Jhikhu Khola catchment[22] (Fig. 3c).

The ratio between calculated water storage variations (Table 1) and water table depth observed here indicates low porosity values of a few percent. We conclude from low porosity values[23], confined behavior[21] and characteristic diffusivity values[8], that the aquifer is predominantly fractured basement. Average water table variation (total annual storage capacity divided by rock porosity, considering low porosity value) is estimated to a few tens of meters in the studied catchments.

We show that the very specific climatic regime of Nepal, characterized by distinct long lasting wet and dry seasons and a major increase of precipitation during ISM (Fig. 1b and 3a), is responsible for the recharge of fractured basement aquifers. The aquifers are refilled during ISM and purged in post-ISM, leading to the annual hysteresis effect that we observed. This behavior is observed in all the studied drainage basins, independent of their size, physiographic location or main basement geology (Fig. 1, Table 1 and Supplementary Figure S6). Very little is known in Nepal about the actual aquifer, its physical properties and the relationship with tectonic structures. These appear as critical unknowns to go further into our understanding of deep groundwater influence on the Himalayan hydrological cycle, including water resources and flood hazard as well as on landslide risk due to pore-pressure saturation processes. Finally, it is noticeable that during winter (December to February) the precipitation-discharge graphs (Fig. 2b) show a systematic higher baseflow for glaciated catchments compared to unglaciated ones. Because glaciers represent an additional water storage component in some catchments, this vertical shift of the hysteresis loops of glaciated catchments reveals the contribution of glacial melt (and snow in spring) to river discharge and can be used to quantify it. From this approach (see Methods), the snow and glacier melt contribution to river discharge is estimated to be ~14±7 km^3 yr^{-1} considering the three main catchments in Nepal (Table 1), which accounts for ~10% of annual river discharge. In Nepal, the volume of water flowing through fractured basement aquifer is approximately 6 times higher than the contribution of glacial and snow melt to river discharge.

Methods

Data and data processing

Precipitation is calculated using APHRODITE (Asian Precipitation Highly Resolved Observational Data Integration Towards Evaluation of Water Resources) data (http://www.chikyu.ac.jp/precip/). Here, we use the daily version for monsoon Asia APHRO_MA_V1003R1, with a spatial resolution of 0.25° [24]. It is currently the best available dataset for Nepal[10]. We use raw river discharge data provided by the Department of Hydrology and Meteorology of Nepal DHM (see e.g. ref. 14), derived from daily stage readings and calibrated rating curves (no interpolated data are used). Potential evapotranspiration is estimated using an elevation-based model developed for Nepal[17]. Basin-wide snow cover is obtained from MOD10C2 version 5 (http://nsidc.org/data/mod10c2v5.html), with an 8-day temporal and 500m spatial resolution[27]. We used the monthly temperature dataset CRU TS3.0[26], with 0.5° gridded resolution. Daily temperature is obtained from linear interpolation.

Baseflow recession analysis

Recession curves have been analyzed for time-series of at least 60 days, where daily rainfall is below potential evapotranspiration and cumulated rainfall < 25 mm for each recession curve. The first 15 days of each recession are not considered when fitting the recession model. Both linear and non linear models are fitted to the relationship between river discharge Q and storage S: $Q=aS^b$. Analytically, exponent b changes from 1 when transmissivity is constant over time (most likely for confined or very deep unconfined aquifers) to 2 for unconfined flow[21]. Coefficient a is the inverse of the response time when b~1.

The annual snow and glacier melt contribution is estimated from the baseflow offset between glaciated and non-glaciated basins along the discharge axis of the hysteresis plots (Fig. 2b). The scatter of baseflow within unglaciated basins (~5 mm/month) is considered as uncertainty. For the Mt. Everest region (here, Dudh Koshi, station 670), our estimated melt volume (0.6 km^3 yr^{-1}, Tab. 1) is consistent with independent glacier mass-loss estimates, measured on ~10% of the glaciated area using satellite altimetry[30].

Hydrological modeling

We consider parsimonious conceptual models at daily and monthly time scales, GR4J and GR2M (http://www.cemagref.fr/webgr/IndexGB.htm). The initial versions have been built up on 4 and 2 parameters respectively. We added a distributed snow module based on the HBV conceptual approach[20]. Data scarcity and requirement of a parsimonious model structure prevented application of a more complex approach. Rainfall and temperature data are redistributed on the ETOPO2v2 (2" resolution) elevation grid. Tsep parameter separates rainfall and snowfall (Supplementary Figure S3). Fusion temperature (T_f) is set to 0°C. Snowmelt (S_m) is driven by a degree-day approach with a constant melting factor M, $S_m=M(T-T_f)$. The snow module adds 2 parameters to the initial GR2M and GR4J models for the whole basin. Modeled snow cover fractions are validated on MODIS snow cover[27] extent ($r^2=0.8$).

The modified GR2M is based on 3 storage compartments; the snow storage, soil store and routing store, interpreted as "groundwater storage" (Supplementary Figure S3). Liquid rainfall and snowmelt are partitioned into excess rainfall, actual evapotranspiration, slow percolation and water remaining in the soil store based on a single parameter. Actual ET is driven by potential ET and reservoir water availability. At monthly time scales, the routing store gathers all water and computes discharge. The model discharge calculation was modified on a physical basis to include a-priori linear behavior from recession curve analysis with variable time response X5, Q=R/X5. GR models allow water exchanges with outside the basin (e.g. subsurface flow) computed with parameter X2. A first order estimate of groundwater flux contribution to river discharge is computed tracking water flow from the routing store of GR4J model.

Modulation of hysteresis effect: Influence of precipitation undercatch, snow melt, reservoir residence time and glacier melt on the shape of hysteresis loops

The shape of the hysteresis curve is used to deduce catchment groundwater storage capacity. Forward modeling studies allow stepwise interpretation of the hysteresis shape with respect to hydrological processes or observation errors, which might have the potential to explain the hysteresis effect. The Rapti catchment (station 360 unglaciated, with no snow) is considered as a reference to test the cumulative impact of several contributions.

We tested:

1) The effect of a systematic underestimation of precipitation and snow on the shape of the hysteresis loop. Applying 30% of excess rainfall[10] shrinks the hysteresis along the precipitation axis (Fig. S5 a).

2) The impact of snow storage and delayed melting contribution to discharge, using GLDAS-NOAH model output[25] as a realistic a priori estimate (100 mm snow per year). Snow melt contribution drags the baseflow upward (in March, April and June) but does not change the general shape of the hysteresis loop (Fig. S5 a).

3) The effect of t_c on the shape of hysteresis loops. The decrease of t_c from ~45 to 10 days, and the associated decrease of the storage capacity, does not allow to reproduce the hysteresis loops observed (Fig. S5 c).

4) The effect of glacier melt on the shape of hysteresis loops. We considered glacier melt contribution at a constant rate and following a seasonal temperature cycle. It induces a year long vertical shift of the hysteresis curve (increased baseflow), keeping its shape intact (Fig. S5 b).

References

1. Alley, W.M., Healy, R.W., LaBaugh, J.W. & Reilly, T.E. Flow and storage in groundwater systems. *Science* **296**, 1985-1990 (2002).

2. Oki, T. & Kanae, S. Global hydrological cycles and world water resources. *Science* **313**, 1068-1072 (2006).

3. Bookhagen, B. & Burbank, D.W. Toward a complete Himalayan hydrological budget: Spatiotemporal distribution of snowmelt and rainfall and their impact on river discharge. *J. Geophys. Res.* **115**, 1-25 (2010).

4. Scherler, D., Bookhagen, B. & Strecker, M.R. Spatially variable response of Himalayan glaciers to climate change affected by debris cover. *Nature Geosci.* **4**, 156-159 (2011).

5. Anderson, S.P., Dietrich, W.E. & Brimhall, G.H. Weathering profiles, mass-balance analysis, and rates of solute loss: Linkages between weathering and erosion in a small, steep catchment. *Geol. Soc. of Am. Bull.* **114**, 1143-1158 (2002).

6. Tipper, E. et al. The short term climatic sensitivity of carbonate and silicate weathering fluxes: Insight from seasonal variations in river chemistry. *Geochim. Cosmochim. Acta* **70**, 2737-2754 (2006).

7. Calmels, D. et al. Contribution of deep groundwater to the weathering budget in a rapidly eroding mountain belt, Taiwan. *Earth Planet. Sci. Lett.* **303**, 48-58 (2011).

8. Montgomery, D.R. & Manga, M. Streamflow and water well responses to earthquakes. *Science* **300**, 2047-2049 (2003).

9. Barros, A.P., Chiao, S., Lang, T.J., Burbank, D. & Putkonen, J. From weather to climate-Seasonal and interannual variability of storms and implications for erosion processes in the Himalaya. *Geol. Soc. Am. Spec. Pap.* **2398**, 17–38 (2006).

10. Andermann, C., Bonnet, S. & Gloaguen, R. Evaluation of precipitation data sets along the Himalayan front. *Geochem. Geophys. Geosys.* **12**, Q07023 (2011).

11. Shrestha, M.L. Interannual variation of summer monsoon rainfall over Nepal and its relation to Southern Oscillation Index. *Meteorol. Atmosph. Physics* **75**, 21-28 (2000).

12. Bookhagen, B., Thiede, R. & Strecker, M. Abnormal monsoon years and their control on erosion and sediment flux in the high, arid northwest Himalaya. *Earth Planet. Sci. Let.* **231**, 131-146 (2005).

13. Immerzeel, W., Droogers, P., Dejong, S. & Bierkens, M. Large-scale monitoring of snow cover and runoff simulation in Himalayan river basins using remote sensing. *Remote Sens. Environ.* **113**, 40-49 (2009).

14. Hannah, D., Kansakar, S., Gerrard, A. & Rees, G. Flow regimes of Himalayan rivers of Nepal: nature and spatial patterns. *J. Hydrol.* **308**, 18-32 (2005).

15. Bookhagen, B. & Burbank, D.W. Topography, relief, and TRMM-derived rainfall variations along the Himalaya. *Geophys. Res. Lett.* **33**, 1-5 (2006).

16. Putkonen, J.K. Continuous Snow and Rain Data at 500 to 4400 m Altitude near Annapurna, Nepal, 1999–2001. *Arctic, Antarctic, and Alpine Research* **36**, 244-248 (2004).

17. Lambert, L. & Chitrakar, B. Variation of potential evapotranspiration with elevation in Nepal. *Mountain Research and Development* **9**, 145–152 (1989).

18. Mouelhi, S., Michel, C., Perrin, C. & Andreassian, V. Stepwise development of a two-parameter monthly water balance model. *J. Hydrol.* **318**, 200-214 (2006).

19. Wang, Q.J. et al. Monthly versus daily water balance models in simulating monthly runoff. *J. Hydrol.* **404**, 166-175 (2011).

20. Bergström, S. *The HBV Model. Computer models in watershed hydrology. V. P. Singh ed.***,** 443-476 (Water Resources Publications: Colorado, USA, 1995).

21. Wittenberg, H. Baseflow recession and recharge as nonlinear storage processes. *Hydrol. Processes* **13**, 715-726 (1999).

22. Dongol, B.S. et al. Shallow groundwater in a middle mountain catchment of Nepal: quantity and quality issues. *Env. Geol.* **49**, 219-229 (2005).

23. De Marsily, G. *Quantitative Hydrogeology: Groundwater Hydrology for Engineering*. (Academic Press: Orlando, 1986).

24. Yatagai, A. et al. A 44-year daily gridded precipitation dataset for Asia based on a dense network of rain gauges. *Sola* **5**, 137–140 (2009).

25. Rodell, M. et al. The Global Land Data Assimilation System. *Bulletin of the American Meteorol. Soc.* **85**, 381-394 (2004).

26. Mitchell, T.D. & Jones, P.D. An improved method of constructing a database of monthly climate observations and associated high-resolution grids. *Int. J. Clim.* **25**, 693-712 (2005).

27. Hall, D.K., Riggs, A.G. & Salomonson, V.V. MODIS/Terra Snow Cover 8-Day L3 Global 0.05deg CMG V005, MOD10C2. Boulder, Colorado USA: National Snow and Ice Data Center. *Digital media* (2006 updated daily).

28. National Snow and Ice Data Center. World glacier inventory. World Glacier Monitoring Service and National Snow and Ice Data Center/World Data Center for Glaciology, Boulder, CO. Digital media. (1999 updated 2009).

29. Department of Mines and Geology Nepal. Geological Map of Nepal. 1:1.000.000 (1994).

30. Bolch, T., Pieczonka, T. & Benn, D.I. Multi-decadal mass loss of glaciers in the Everest area (Nepal Himalaya) derived from stereo imagery. *The Cryosphere* **5**, 349-358 (2011).

Acknowledgements

C.A. benefited from a 3 years PhD scholarship awarded by the German Academic Exchange Service (DAAD, D/08/42538) and from the French-German double PhD program of the French-German University Saarbrücken (DFH/UFA). The authors like to thank K. P. Sharma and his team from the Department of Hydrology and Meteorology of Nepal (DHM) for providing hydrological data and M. Dhakal from ICIMOD Nepal for sharing supplementary information on dug-well measurements.

Authors contributions

C.A. acquired and analyzed the data. L.L. and C.A. performed the hydrological modeling. All authors discussed the results and wrote the manuscript.

Additional information

Correspondence and requests for materials should be addressed to C.A.

Figure captions

Figure 1| Hydrological setting of the Nepal Himalayas. a, Precipitation distribution map, hydrological discharge stations used in this study (black diamonds) and contours (red lines) of the studied drainage basins. Grey lines mark political boundaries. Mean annual precipitation rates (see

methods), representing 50 years of data, are draped over shaded relief. River network is displayed in blue and glaciers in white (after ref. 28). **b,** Mean basin-wide precipitation (1951-2006, in green), discharge (blue) and potential evapotranspiration (red) for the Narayani drainage basin. Bold blue line with blue shading represents the mean, maximum and minimum daily discharge over 34 years (station 450). **c,** Simplified geological map of Nepal[29]: QS: Quaternary Sediments, SW: Siwaliks formation, LH: metasediments of the Lesser Himalayas, HCC: High Himalayan Cristalline, TSS: Tethyan Sediment Series.

Figure 2| Precipitation-discharge (P-Q) anticlockwise hysteresis plot. a, Bi-logarithmic P-Q plot of daily data for the Narayani basin over 34 years at station 450 (~12,300 data points). Data plotted are specific discharges (discharges normalized by drainage area) and mean basin precipitation rates. Note that discharge is not plotted when precipitation is zero. Color bar is scaled for a calendar year. White filled circles represent the mean monthly values over 34 years, the months being indicated by numbers. The error bars represent the 5% and 95% quantiles of the daily data distribution of each month. Inset shows the data filtered with a 30-day moving average. **b,** Mean annual hysteresis loops plotted from monthly mean data for all the drainage basins. Solid lines represent partially glaciated basins and dashed lines unglaciated ones (percentage of glacial coverage from ref. 28).

Figure 3| 10-year (1997-2006) temporal variability of several hydrological compartments, Narayani basin. **a,** Daily precipitation (green), and daily specific river discharge (blue). **b,** Temperature (orange) as a glacier melt proxy (from CRU[26]) and percentage of basin-wide snow cover (dark green, data from MODIS MOD10C2 v.5[27] with a 8-day temporal resolution). **c,** Calculated groundwater storage (red), shading illustrating model uncertainty (Supplementary Figure S2). Ground water table variation (dark blue) observed in a dug-well in Jhikhu Khola Basin[22] (station no. 1) from ref. 22 and unpublished data provided by these authors. The abnormal low water table in 2004 likely results from exhaustive exploitation.

Table 1| Properties of the studied drainage basins and summary of results (monthly modeling). Maximum elevation is used as a proxy for snow occurrence during winter (considering winter snowline at ~3000 m asl.[16]). Precipitation rate is computed as a mean basin value. Specific discharge is computed from daily river gauge data. Real-evapotranspiration ETR is computed from our modeling (see Methods). Storage represents the mean annual amplitude of storage variation and its respective uncertainty in km³ and mm respectively (Supplementary Figure S2). t_c is the characteristic basin response time, derived from hydrological modeling or from the recession curve of hydrographs (see Methods). The % glaciated values are calculated using data from ref. 28. Ice melt is the annual volumetric glacier ice melt contribution to the rivers, estimated from the relative baseflow shift in the precipitation-discharge plot (Fig. 2b). % snow-melt is the contribution of snow to discharge (both directly and via the aquifer).

Supplementary Figure

S1| Difference between strong and weak monsoon hysteresis loops. Precipitation-discharge hysteresis loop for the strong monsoon year 1999 and the weak monsoon year 1997[11] for the Narayani Basin. Data has been filtered with a 5-day moving average to avoid small-scale noise. The amplitude of the hysteresis loop is larger during strong monsoon years compared to weak ones. Q/A is the specific discharge, P is the mean basin precipitation.

S2| 10-year (1997-2006) temporal variability of several hydrological discharge cycle compartments, Koshi Basin (I) and Karnali Basin (II), central Nepal. a, Daily precipitation (green), and daily specific river discharge (blue). **b**, Temperature (orange) as a glacier melt proxy (from CRU[26]) and percentage of basin-wide snow cover (dark green, data from MOD10C2 v.5[27] with an 8-day temporal resolution). **c**, Calculated groundwater storage evolution (red) derived from a modified version of the conceptual hydrological model GR2M[18] (see methods), shading illustrating model uncertainty, and ground water table variation (dark blue) observed in dug-wells in the Jhikhu Khola Basin[22] (station no. 1).

Uncertainty estimation:

A Monte-Carlo approach is carried out to quantify the impact of observation data uncertainties on modeled groundwater properties (storage capacity, response time, see Table 1). Multiplicative errors have been considered for rainfall and discharge. Rainfall might be systematically underestimated by 30%10, and discharge biased by ±5%. Conversely, ET and temperature errors are taken as additive, based on differences between independent datasets. Model is then recalibrated, model structure error is therefore not considered in this uncertainty analysis. While groundwater storage capacity is highly sensitive to systematic bias in precipitation data, recession curves, and therefore time response, are rather well constrained (Table 1).

S3| Flowchart of the modified version of the conceptual hydrological model used in this study. Simplified schema of the conceptual models GR2M and GR4J[18], and the added snow module. Black lines applied for both models GR2M and GR4J whereas gray dotted lines applied only for model GR4J. Please refer to Mouelhi et al. 2006 (ref. 18), the method section and the following web resource http://www.cemagref.fr/webgr/Modelesgb/descriptionsgb.htm for more detailed information.

S4| Modeled vs. observed hysteresis loop for Narayani catchment (450). Data are plotted on a monthly scale. The inset shows the linear correlation between the observed and modeled discharge. Q/A is the specific discharge. P is the monthly basin-wide precipitation rate.

S 5| Influence of precipitation undercatch, snow melt, reservoir residence time and glacier melt on the shape of hysteresis loops. The months are indicated by numbers. In all the examples, the mean monthly precipitation-discharge values for Rapti River at station 360 are used as a reference (blue). **a,** Effect of a constant 30% undercatch of precipitation and impact of snowmelt contribution, considering an annual water equivalent of the snowmelt contribution after the GLDAS-NOAH model[25] (inset). **b,** Impact of the basin-wide storage capacity on the hysteresis shape of the Rapti catchment, considering characteristic basin response times of 35 days and of only 10 days, corresponding to a 20-fold downsizing of the storage capacity (see Methods). **c,** Influence of a 100 mm yr^{-1} glacier melt

403 contribution (or storage), considering a constant melt rate, equally distributed over the whole year or
404 assuming a cyclic, temperature-driven ice melt contribution (both illustrated in the inset).
405
406 **S6 | Comparison between groundwater storage properties and geological units within the studied**
407 **drainage basins.** Graphs illustrate storage properties (response time and storage capacity), plotted
408 against geological unites.
409
410 **Table S1| Properties of the studied drainage basins and summary of results (daily modeling)**.
411 Real-evapotranspiration ETR, is computed from the conceptual model GR4J[18] on the basis of potential
412 evapotranspiration[17]. The storage represents the mean annual amplitude of storage variation and its
413 respective uncertainty (Supplementary Figure S2), in km³ and mm respectively. t_c is the characteristic
414 basin response time derived from the model GR4J and the recession curve of the falling limp of the
415 hydrographs. % snow-melt is the contribution of snow to discharge (both directly and via the aquifer).
416 The retarded discharge represents groundwater contribution to the river discharge and is expressed as
417 percent of the annual river discharge.

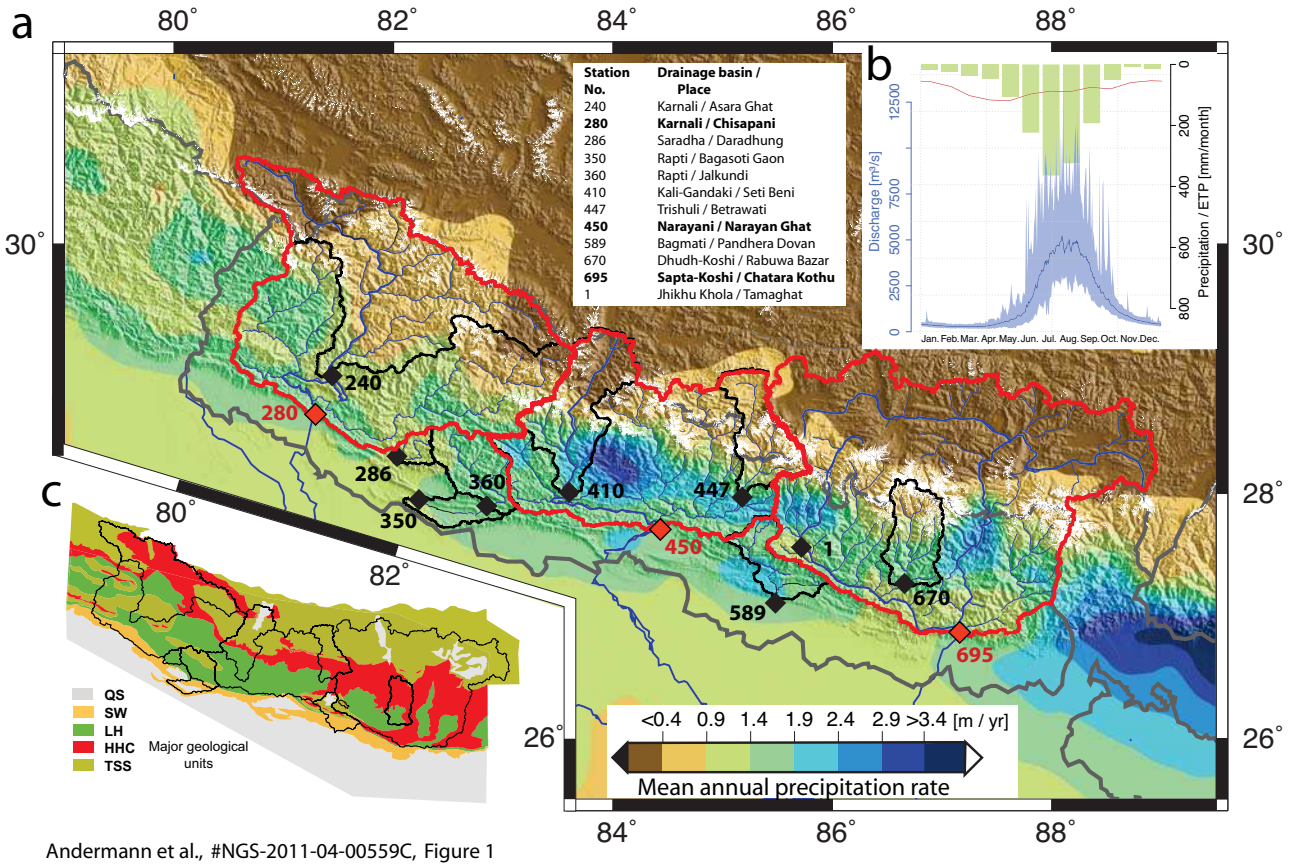

Andermann et al., #NGS-2011-04-00559C, Figure 1
Two columns, 170 mm large

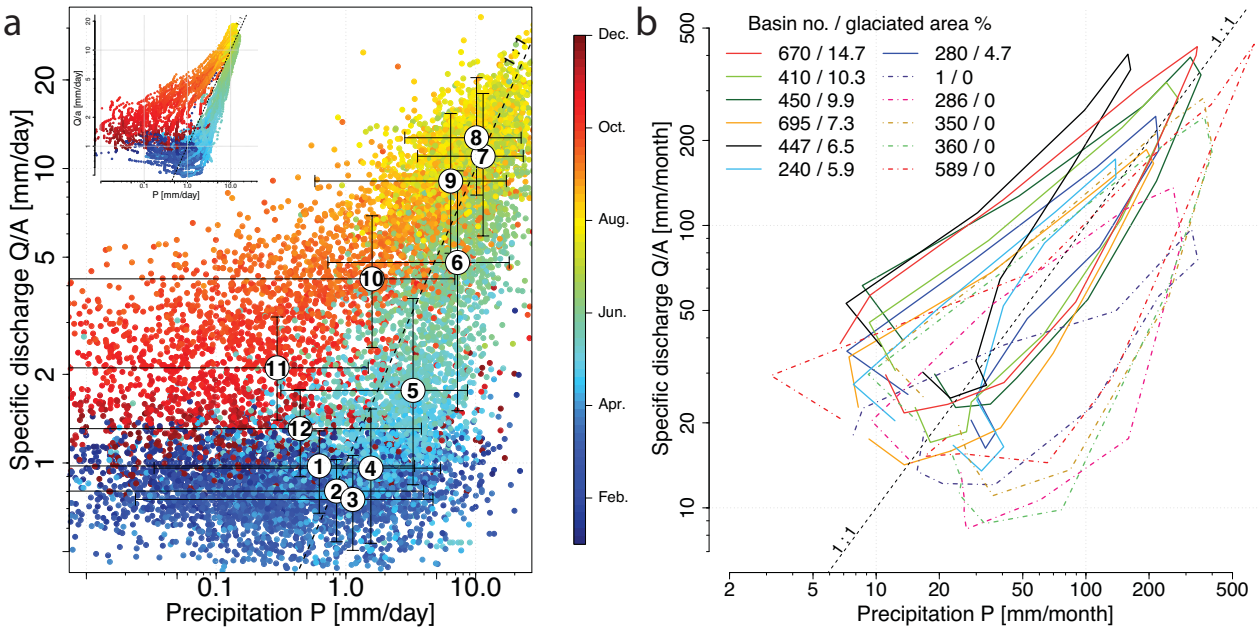

Andermann et al., #NGS-2011-04-00559C, Figure 2
Two columns, 170 mm large

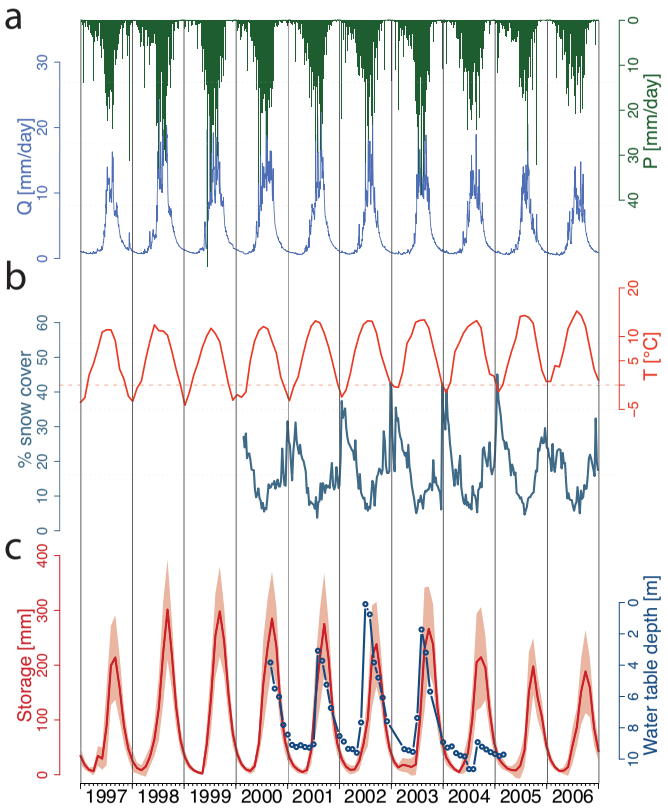

Andermann et al., #NGS-2011-04-00559C, Figure 3
One columns, 88 mm large

Station No.	240	**280**	286	350	360	410	447	**450**	670	**695**	589	1
Basin	Karnali	**Karnali**	Saradha	Rapti	Rapti	Kali Gandaki	Trishuli	**Narayani**	Dudh Koshi	**Sapta Koshi**	Bagmati	Jhikhu Khola
Lat [°]	28.95	**28.64**	28.64	27.90	27.95	28.01	27.97	**27.71**	27.27	**26.87**	27.11	27.59
Long [°]	81.44	**81.29**	82.03	82.85	82.23	83.60	85.18	**84.43**	86.66	**87.16**	85.48	85.67
Size [km²]	21121	**45967**	808	3648	5198	7169	4428	**32002**	3880	**57719**	2849	111
Precipitation [mm yr^{-1}]	558	**920**	1107	1522	1470	1030	692	**1396**	1295	**920**	1932	1285
Discharge [mm yr^{-1}]	650	**789**	460	903	787	1145	1513	**1145**	1598	**1039**	1205	374
ETR [mm yr^{-1}]	176	**234**	656	720	654	178	121	**367**	178	**179**	839	171
Availability of discharge	1975-2006	**1973-2006**	1976-2006	1978-2006	1985-2006	1979-1995	1977-2006	**1973-2006**	1987-2006	**1977-2006**	2001-2006	1998-2006
%Area glaciated	5.9	**4.7**	0.0	0.0	0.0	10.3	6.5	**9.9**	14.7	**7.3**	0.0	0.0
Max Elevation [m asl.]	7549	**7697**	2800	3623	3623	8147	7352	**8147**	8848	**8848**	2795	2200
Nash-Sutcliffe coef.	0.93	**0.92**	0.79	0.88	0.95	0.91	0.79	**0.91**	0.94	**0.89**	0.88	0.29
Recession exp. *b* ($Q=aS^b$)*	1.01	**1.11**	1.16	1.01	1.18	1.01	1.02	**1.16**	1.17	**1.01**	1.12	1.18
Storage capacity [km³]	3.1 ±1.2	**8.1 ±3.3**	0.21 ±0.08	1.6 ±0.7	1.8 ±0.8	1.3 ±0.6	0.9 ±0.4	**9.9 ±3**	1.2 ±0.4	**10.3** ±6	1.2 ±0.5	0.03 ±0.01
Storage capacity [mm]	150±60	**175**±70	260±90	430±180	350±150	180±80	200±80	**310**±125	300±105	**180**±100	440±180	300±120
t_c GR2M [days]*	46 ±5	**50** ±5	37 ±3	36 ±8	41 ±8	45 ±4	38 ±4	**50** ±5	53 ±11	**47** ±4	30 ±5	120 ±35
t_c recession curve [days]*	40 ±10	**46** ±15	37 ±13	44 ±17	42 ±15	41 ±15	44 ±11	**40** ±13	45 ±9	**41** ±11	41 ±19	77 ±24
Ice+snow melt [km³ yr^{-1}]	1.2	**4.1**	n.a.	n.a.	n.a.	0.7	0.8	**5.3**	0.6	**4.1**	n.a.	n.a.
% snow-melt	12	**7**	n.a.	n.a.	n.a.	3	13	**2**	6	**5**	n.a.	n.a.
Geology units % coverage QS/SW/LH/HHC/TSS	0/0/17/44/39	**0/5/33/25/37**	0/3/96/0/1	0/5/62/0/33	8/24/45/0/23	10/0/32/15/43	0/0/8/37/55	**2/0/42/23/33**	0/0/26/73/1	**6/0/16/40/38**	13/42/2/11/32	0/0/11/17/72

* see Methods